nature synthesis

Article

https://doi.org/10.1038/s44160-023-00292-9

Catalytic production of ammonia from dinitrogen employing molybdenum complexes bearing N-heterocyclic carbene-based PCP-type pincer ligands

Received: 31 May 2022

Accepted: 15 March 2023

Published online: 17 April 2023

Check for updates

Yuya Ashida[1], Takuro Mizushima[1], Kazuya Arashiba[1], Akihito Egi[2], Hiromasa Tanaka[3], Kazunari Yoshizawa[2] ✉ & Yoshiaki Nishibayashi[1] ✉

Mechanistic insight into the catalytic production of ammonia from dinitrogen is needed to improve the synthesis of this vital molecule. Here we study the use of samarium diiodide (SmI_2) and water in the presence of molybdenum complexes that bear PCP-type pincer ligands to synthesize ammonia. The proton-coupled electron transfer during the formation of a N–H bond on the molybdenum imide complex was found to be the rate-determining step at high catalyst concentrations. Additionally, the dimerization step of the catalyst became the rate-determining step at low catalyst concentrations. We designed PCP-type pincer ligands with various substituents at the 5- and 6-positions and observed that electron-withdrawing groups promoted the reaction rate, as predicted by density functional theory calculations. A molybdenum trichloride complex that bears a trifluoromethyl group functioned as the most effective catalyst and produced up to 60,000 equiv. ammonia based on the molybdenum atom of the catalyst, with a molybdenum turnover frequency of up to 800 equiv. min^{-1}. The findings reported here can contribute to the development of an environmentally friendly next-generation nitrogen-fixation system.

Ammonia plays an essential role globally as a raw material to produce fertilisers and nitrogen-containing materials, which include pharmaceuticals, plastics, textiles and explosives. Presently, the Haber–Bosch process, with which ~144 metric tonnes of nitrogen are converted into ammonia annually, accounts for the main method to synthesize ammonia at the industrial level[1]. However, the conversions of dinitrogen and dihydrogen gases into ammonia via the Haber–Bosch process require a high temperature and pressure. Additionally, the preparation of dihydrogen feedstocks consumes a substantial amount of fossil fuels and is accompanied by considerable carbon dioxide (CO_2) emission[2,3]. Ammonia recently attracted attention as a candidate transporter of sustainable energy because of its ease of liquefication, which is suitable for storage and transportation; moreover, only water and dinitrogen gas are emitted via combustion[4–6]. Thus, the past decade witnessed a demand for an environmentally friendly and tractable production of ammonia[7,8]. Notably, extensive studies were conducted on nitrogen fixation catalysed by heterogeneous catalysts to achieve the production of ammonia at a low temperature and pressure[9–12].

Since the breakthrough reported by Yandulov and Schrock, the development of nitrogen fixation under mild reaction conditions in the

[1]Department of Applied Chemistry, School of Engineering, The University of Tokyo, Tokyo, Japan. [2]Institute for Materials Chemistry and Engineering, Kyushu University, Fukuoka, Japan. [3]School of Liberal Arts and Sciences, Daido University, Nagoya, Japan. ✉e-mail: kazunari@ms.ifoc.kyushu-u.ac.jp; ynishiba@g.ecc.u-tokyo.ac.jp

https://doi.org/10.1038/s44160-023-00292-9

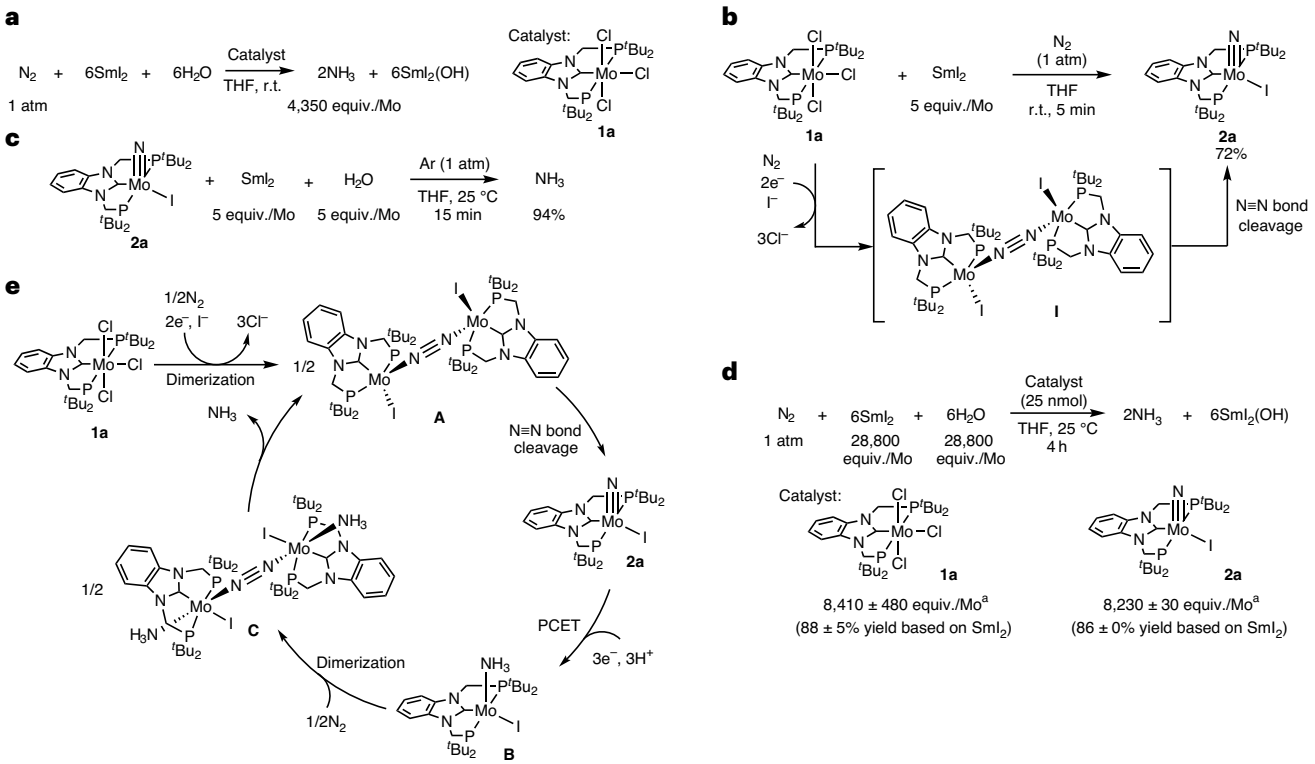

Fig. 1 | Stoichiometric and catalytic reactions that employ molybdenum complexes bearing PCP-type pincer ligands. a, Previously reported catalytic reaction[30]. **b**, Stoichiometric reduction of **1a** with an excess amount of SmI_2 in a dinitrogen atmosphere. **c**, Stoichiometric reaction of **2a** with excess amounts of SmI_2 and H_2O in an argon atmosphere. **d**, Catalytic reduction of dinitrogen with large amounts of SmI_2 and H_2O in the presence of the molybdenum complexes as the catalysts. **e**, Plausible reaction pathway for **1a** and **2a**. [a]Data are the mean of the multiple individual experiments (a minimum of two), and the error bars represent the standard deviation (s.d.). r.t., room temperature.

presence of transition metal complexes (as homogeneous catalysts) has progressed exceptionally[13]. Employing the homogenous catalytic reaction system, dinitrogen gas can be converted into ammonia by reactions with reductants and proton sources (as the chemical reagents) in the presence of a catalytic amount of transition metal complexes as the catalysts at atmospheric pressure or room temperature or lower, for example, −78 °C (refs. 14–17). At the early stage of these reactions, the system often exhibited a limited catalytic activity owing to the deactivation of the catalysts and/or formation of dihydrogen as a side product from the high reactivity of the reductants, as well as the proton sources[13,18–28]. Very recently, we reported the catalytic formation of ammonia from dinitrogen gas by combining samarium diiodide (SmI_2) with water (as the one-electron reductant and the proton source, respectively) in the presence of molybdenum complexes that bear a N-heterocyclic carbene (NHC)-based PCP-type pincer ligand under ambient reaction conditions[29] (Fig. 1a)[30]. Our reaction system exhibited a high catalytic activity, and demonstrated a high production of ammonia; the amount of ammonia produced reached 4,350 equiv. based on the molybdenum atom of the catalysts (the turnover frequency (TOF) was ~120 min^{-1}).

Here we designed molybdenum complexes that bear different substituted PCP-type pincer ligands based on experiments, which included the isolation of nitride complexes as key reactive intermediates, as well as kinetic and theoretical studies of the catalytic reaction. Thereafter, we investigated the catalytic activity of the molybdenum complexes in the production of ammonia under ambient reaction conditions with SmI_2 and water as the reductant and the proton source, respectively. Ultimately, our system dramatically increased the quantity of ammonia produced, as well as the reaction rate, compared with the results of our previous study[30].

Results and discussion

Preparation and reactivity of the molybdenum–nitride complex

In our previous study, which was based on the stoichiometric and catalytic reactions of molybdenum(III) trihalide complexes that bear a pyridine-based PNP-type pincer ligand, [MoX_3(PNP)] (X = Cl, Br and I)—in which the corresponding molybdenum(IV)–nitride complex [Mo(≡N)I(PNP)] was a key reactive intermediate in the catalytic formation of ammonia under ambient reaction conditions—the molybdenum(III) trichloride complex that bears the NHC-based PCP-type pincer ligand [$MoCl_3$(PCP)] (**1a**; PCP = 1,3-bis((di-*tert*-butylphosphino)methyl) benzimidazol-2-ylidene) exhibited an excellent catalytic activity[30]. However, the corresponding molybdenum(IV)–nitride complex that bears the NHC-based PCP-type pincer ligand [Mo(≡N)I(PCP)] (**2a**) was not prepared.

Therefore, we first prepared **2a** in this study following the same procedure as that to prepare [Mo(≡N)I(PNP)]. The reaction of **1a** with 5 equiv. SmI_2 in atmospheric dinitrogen and THF for five minutes at room temperature (25 °C) afforded **2a** in a 72% NMR yield (Fig. 1b). Next, via the reaction of [MoI_3(PCP)] with KC_8 as a reductant, we isolated the nitride complex (**2a**) as a pure form. The detailed molecular structure of **2a** was confirmed via X-ray analysis (Supplementary Fig. 7). This experimental result, which is illustrated in Fig. 1b, indicated that the transformation of **1a** into **2a** proceeded via the N≡N bond cleavage of a dinitrogen-bridged Mo(I)–N≡N–Mo(I) complex (**I**) after a two-electron reduction and ligand exchanges of **1a**. We previously carried out a kinetic study on the stoichiometric reaction of [MoI_3(PNP)] with SmI_2 to give [Mo(≡N)I(PNP)] via a dinitrogen-bridged dimolybdenum(I) complex [MoI(PNP)]–N≡N–[MoI(PNP)] (ref. 30). This experimental result indicates that the stoichiometric transformation of [MoI_3(PNP)]

https://doi.org/10.1038/s44160-023-00292-9

into [Mo(≡N)I(PNP)] proceeded via a dinuclear complex, such as the dinitrogen-bridged dimolybdenum complex as a key reactive intermediate[31]. In addition, we more recently investigated cycling between molybdenum(I)–dinitrogen and molybdenum(IV)–nitride complexes to support our proposed reaction pathway for the catalytic formation of ammonia from dinitrogen, together with density functional theory (DFT) calculations[32]. Based on our previous results, here we quantitatively confirmed the conversion of the nitride ligand in **2a** into ammonia via the reaction of **2a** with 5 equiv. SmI_2 and H_2O in an argon atmosphere and THF for 15 minutes at 25 °C (Fig. 1c). These experimental results indicated that dinitrogen can be transformed into ammonia employing **2a** as a reactive intermediate.

Next, we compared the catalytic activities of **1a** and **2a** in ammonia formation under the optimized reaction conditions (Fig. 1d). The reaction of dinitrogen (1 atm) with 28,800 equiv. SmI_2 (the reductant) and 28,800 equiv. H_2O (the proton source) in the presence of a catalytic amount (25 nmol) of **1a** in THF for four hours at 25 °C yielded 8,410 equiv. ammonia based on the molybdenum atom of the catalyst (88% yield based on SmI_2). The catalytic reaction that employed **2a** rather than **1a** as the catalyst exhibited almost the same catalytic activity. Based on these stoichiometric and catalytic reactions, we expected that the molybdenum(IV)–nitride complex (**2a**) would function as a key reactive intermediate to effectively promote the catalytic nitrogen.

Based on our previous[30–32] and present findings, we proposed the following reaction pathway for the production of ammonia employing **1a** as the precatalyst and **2a** as key reactive intermediate (Fig. 1e): first, the two-electron reduction of **1a** with 2 equiv. SmI_2, as well as the ligand exchange of chloride with the iodide obtained from SmI_2, yields the corresponding dinitrogen-bridged dimolybdenum(I) complex (**A**). Afterwards, the cleavage of the bridged dinitrogen ligand in **A** affords the corresponding molybdenum(IV)–nitride complex (**2a**). Subsequently, **2a** is converted into the corresponding molybdenum(I)–ammonia complex (**B**) via three reduction and protonation steps that employed imide and amide complexes. The proton-coupled electron transfer (PCET) process[33–35] in the reaction of dinitrogen with SmI_2 and H_2O is generally proposed as the key steps[36–38]. After the formation of **B**, its subsequent dimerization facilitates the formation of a six-coordinated **A** (**C**). Finally, the elimination of the ammonia ligand from **C** regenerates **A**, and thereby completes the catalytic cycle. As pointed out in the previous paragraph, this proposed reaction pathway was supported by DFT calculations in the reaction that employed the corresponding molybdenum complexes that bear the PNP-type pincer ligand[32]. We previously investigated the stoichiometric reactions of the molybdenum–nitride complex that bear the PNP-type pincer ligand, [Mo(≡N)I(PNP)], as well as their kinetic isotope effect (KIE)[30]. These experimental results revealed that the transformation of **2a** into **B** also proceeded via PCET.

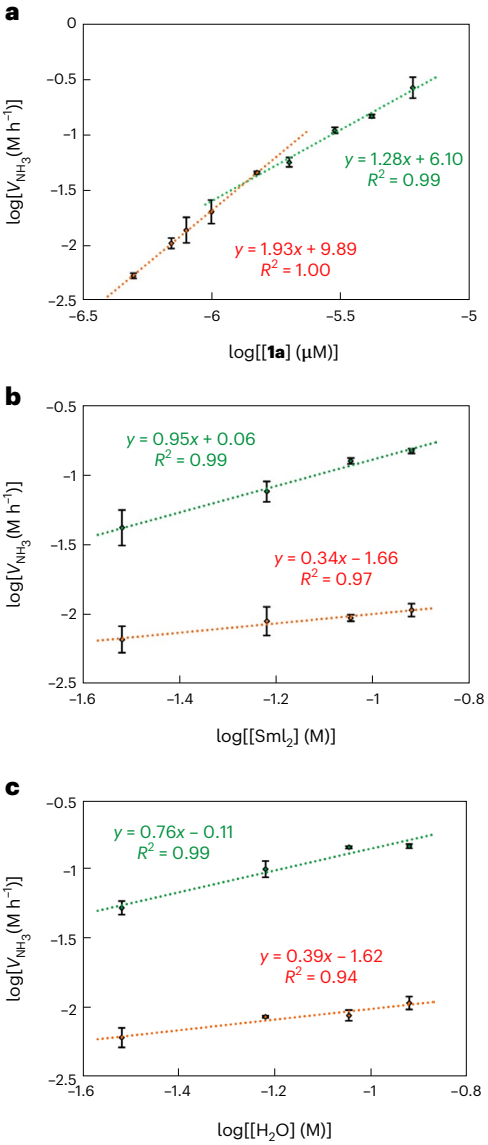

Fig. 2 | Plots of the estimation of the reaction order in each reagent. The green and orange plots and lines represent the data in the presence of high and low concentrations of the catalyst, 1.5 μM < [**1a**] and [**1a**] < 1.5 μM, respectively. Data are the average of two or three experiments with error bars based on s.d. **a**, Plots of log(v_{NH_3}) versus log([**1a**]). **b**, Plots of log(v_{NH_3}) versus log([SmI_2]). **c**, Plots of log(v_{NH_3}) versus log[H_2O].

Kinetic study of the catalytic reaction

To gain more insight into the reaction pathway of the formation of ammonia (Fig. 1e), we determined the kinetic parameters of the catalytic reduction of dinitrogen via the reaction with SmI_2 and H_2O in the presence of **1a** in THF at room temperature. A THF solution that contained SmI_2 (0.12 M) and H_2O (0.12 M) was mixed in atmospheric dinitrogen (1 atm) in the presence of 6–0.5 μM **1a** at room temperature. The initial rate of producing ammonia (v_{NH_3}) was determined, following the ammonia yield from the catalytic reaction that was quenched at the initial stage. The reaction order with respect to **1a** was obtained from the slope of the plot of log(v_{NH_3}) versus log([**1a**]), where [**1a**] is the concentration of **1a** (Fig. 2a). The reaction order exhibited two different kinetic regions based on the concentration of the catalyst. One was the first order, which employed the catalyst at high concentrations (region A, represented by the green line), and the other was the second order, which employed the catalyst at low concentrations (region B, represented by the orange line). Similar phenomena were observed in the ruthenium-catalysed oxidation of water in which the dimerization of the ruthenium complexes was the key step[39,40].

To investigate the rate-determining steps of both regions, we determined the rate orders in the presence of SmI_2 and H_2O at high ([**1a**] = 4.17 μM) and low ([**1a**] = 0.7 μM) concentrations of **1a** (the catalyst). Thus, employing a high concentration of the catalyst (region A), we estimated that SmI_2 and H_2O exhibited first-order kinetics (0.95 and 0.76 for SmI_2 and H_2O, respectively), as estimated for **1a** (Fig. 2b,c, green line). These experimental results indicated that the reaction involving the three molecules, **1a**, SmI_2 and H_2O, was the rate-determining step in region A. Such reaction steps were attributable to the reduction and protonation steps in PCET (Fig. 1e). Conversely, the estimated small rate orders in SmI_2 and H_2O employing a low concentration of the catalyst were not really zeroth order (0.34 and 0.39 for SmI_2 and H_2O, respectively) (Fig. 2b,c, orange line). These small orders may be due to the result of a background reduction of water into dihydrogen[41]. Based on these results, we deduced that only the concentration of the

molybdenum catalyst affected the second-order reaction rate at a low concentration of the catalyst. Thus, at a low catalyst concentration, the dimerization of the molybdenum complexes accounts for the rate-determining step (Fig. 1e).

Further, we measured the kinetic isotope effect of the catalytic reaction with H_2O or D_2O in both concentration regions. A k_H/k_D value of 2.61 was observed in region A; this value confirmed that the PCET process was the rate-determining step[36–38]. Conversely, a k_H/k_D value of 1.42 was observed in region B, although no kinetic isotope effect was predicted by the kinetic study because of the lack of a relationship between the proton sources and the dimerization step of the catalyst as the rate-determining step. Although the details are unclear, the k_H/k_D differences between the two regions are consistent with a change in the rate-determining step at low and high catalyst concentrations.

Density functional theory calculations of the bond dissociation free energies

Next, we employed two strategies, based on the kinetic study (Fig. 2), to improve the catalytic activity of the system by tuning the pincer ligand of the molybdenum catalysts. The first strategy involved accelerating the PCET process in the presence of a high concentration of the catalyst, and the other involved accelerating the dimerization process in the presence of a low concentration of the catalyst. Here we focused on adding hydrogen atoms to the nitride complex (**2a**) to produce an ammine complex (**IIIa**) via PCET, after which we computationally predicted the influence of introducing the substituents to the pincer ligand of **2a** on the thermodynamic stability of the hydrogenated intermediates. We previously reported that the nitrogen-fixing activity of the molybdenum–dinitrogen complexes that bear PNP-type pincer ligands could be tuned by introducing electron-donating and withdrawing groups to the pincer ligands[42,43].

First, we performed the DFT calculations at the B3LYP-D3 theory level[44–48] to evaluate the bond dissociation free energies (BDFEs) of the N–H bonds in three possible reaction intermediates, beginning with **2a**, namely the imide (**Ia**), amide (**IIa**) and ammine (**IIIa**) complexes. BDFEs were calculated according to the reaction [MoI(NH_x)(PCP)] → [MoI(NH_{x-1})(PCP)] + H (x = 1–3); therefore, [MoI(NH_x)(PCP)] lost a proton and an electron simultaneously. Chirik and co-workers utilized the BDFEs of N–H bonds to discuss the photoinduced PCET-driven reductions of different transition-metal–nitrogen complexes, such as manganese–nitride[49,50], titanium–amide[51] and cobalt–imide complexes[51]. In our previous study on the molybdenum-catalysed nitrogen fixation reaction that employed [Mo(N_2)($PMePh_2$)$_4$], the BDFE of the N–H bond of a molybdenum–diazenide (Mo–NNH) complex was employed to evaluate the hydrogen atom affinity[52]. Table 1 lists the calculated BDFE(N–H) values of the three intermediates. The calculated BDFE(N–H) values of [MoI(NH_x)(PCP)] were 33.8, 52.7 and 41.2 kcal mol^{-1} for the imide (x = 1), amide (x = 2) and ammine (x = 3) complexes, respectively. All the calculated BDFE values were comparable with or higher than that of the O–H bond (34 kcal mol^{-1}) of water bound to a Sm(II) centre in THF[41]; thus, the successive addition of hydrogen atoms to **2a** employing H_2O in the presence of SmI_2 was thermodynamically reasonable[53]. The smallest BDFE(N–H) value (that of the imide complex **Ia**) indicated that the addition of the first hydrogen atom (protonation and reduction) was the most energetically unfavourable process in the transformation of the nitride N atom of **2a** into ammonia.

Next, we investigated the influence of the introduction of substituents to the benzimidazole skeleton of the PCP ligand on the BDFEs of [MoI(NH_x)($PCP^{R1,R2}$)] (x = 1–3), where R^1 and R^2 are the substituents at positions 5 and 6 in the benzimidazole skeleton. To obtain the trends in a wide range of the Hammett substituent constants (σ_p) (ref. 54), we examined one electron-donating methyl group (σ_p = −0.17) and three electron-withdrawing groups, namely Cl, F and CF_3 with σ_p values of 0.06, 0.23 and 0.54, respectively. For the CF_3 group, its 5-substituted (R^1 = CF_3, R^2 = H) and 5,6-substituted (R^1 = R^2 = CF_3) PCP ligands were considered. Table 1 summarizes the BDFE(N–H) values of [MoI(NH_x)($PCP^{R1,R2}$)] (x = 1–3). The BDFE(N–H) values of all the substituted complexes exhibited the same trend as those of the unsubstituted ones, in the following order: imide (x = 1) < ammine (x = 3) < amide (x = 2). Therefore, the following discussion focuses on the addition of hydrogen atoms to the nitride complexes to yield the corresponding imide complexes, as this step was the most energetically unfavourable.

Table 1 | BDFE values of the N–H bonds of the imide, amide and ammine complexes that bear the substituted PCP ligands

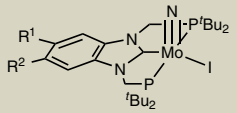

(R^1, R^2)	Hammett substituent constant (σ_p)	BDFE(N–H) (kcal mol^{-1})		
		Imide complex (I)	Amide complex (II)	Ammine complex (III)
(H, H)	0.00	33.8 (**Ia**)	52.7 (**IIa**)	41.2 (**IIIa**)
(Me, Me)	−0.17	32.8 (**Ib**)	52.1 (**IIb**)	40.8 (**IIIb**)
(F, F)	0.06	33.6 (**Ic**)	53.6 (**IIc**)	41.4 (**IIIc**)
(Cl, Cl)	0.23	33.7 (**Id**)	54.7 (**IId**)	41.4 (**IIId**)
(CF_3, H)	0.54	35.8 (**Ie**)	53.2 (**IIe**)	42.8 (**IIIe**)
(CF_3, CF_3)	0.54	35.1 (**If**)	50.9 (**IIf**)	42.3 (**IIIf**)

Based on the BDFE(N–H) results, we examined how the substituted PCP ligands modified the electronic structure of [MoI(N)(PCP)] **2a**. Figure 3a plots the highest occupied molecular orbital (HOMO) and lowest unoccupied molecular orbital (LUMO) energies of **2a** and 5,6-substituted [MoI(N)($PCP^{R1,R2}$)] (**2b**–**2d**, **2f**) versus the σ_p values. Both molecular orbital energy levels correlated with the Hammett substituent constant, and a strong electron-withdrawing substituent, such as $-CF_3$, lowered (or stabilized) the LUMO energy of the nitride complex more effectively than it did the HOMO energy. The lowering of the LUMO energy of **2a** is expected to improve the PCET reaction to yield the corresponding imide complex, as it will enhance the electron affinity of **2a**.

NHCs coordinated to a transition-metal centre are known to serve not only as a strong σ-donor but also as a π acceptor[29,55,56]. As shown in Fig. 3b, the spatial distribution of the LUMO of **2a** delocalizes over the Mo≡N moiety as well as the benzimidazole moiety of the PCP ligand. These moieties are connected through an overlap between the d_{zx} orbital of Mo and the p_z orbital of the carbene C atom of the PCP ligand. Therefore, the electron-donating and withdrawing substituents can affect the strength of the Mo–C(carbene) bond of the substituted imide complexes [MoI(NH)($PCP^{R1,R2}$)] generated by the PCET to give [MoI(N)($PCP^{R1,R2}$)]. Figure 3c plots the Mayer bond orders[57] of the imide complexes **Ia**–**Id** and **If** versus the σ_p values. The strength of the Mo–C(carbene) bond is in good correlation with the σ_p values, and a strong electron-withdrawing substituent, such as $-CF_3$, can strengthen the connection between the Mo centre and the PCP ligand. As depicted in Fig. 3d, the α-HOMO of **1a** in the doublet spin state, which corresponds to the LUMO of **2a**, is responsible for the π backdonation from the singly occupied d_{zx} orbital of Mo to the vacant p_z orbital of the carbene C atom. We previously reported that this unique π-accepting ability of the NHC-based PCP ligand contributed to the high thermodynamic stability of [{Mo(0)(N_2)$_2$(PCP)}$_2$(μ-N_2)] as an N_2-fixing catalyst[29,58]. Therefore, we can expect that the use of the substituted PCP ligands improves the catalytic activity of the present Mo–PCP system for nitrogen fixation.

In summary, DFT calculations predicted that the introduction of strong electron-withdrawing substituents, such as $-CF_3$, to

https://doi.org/10.1038/s44160-023-00292-9

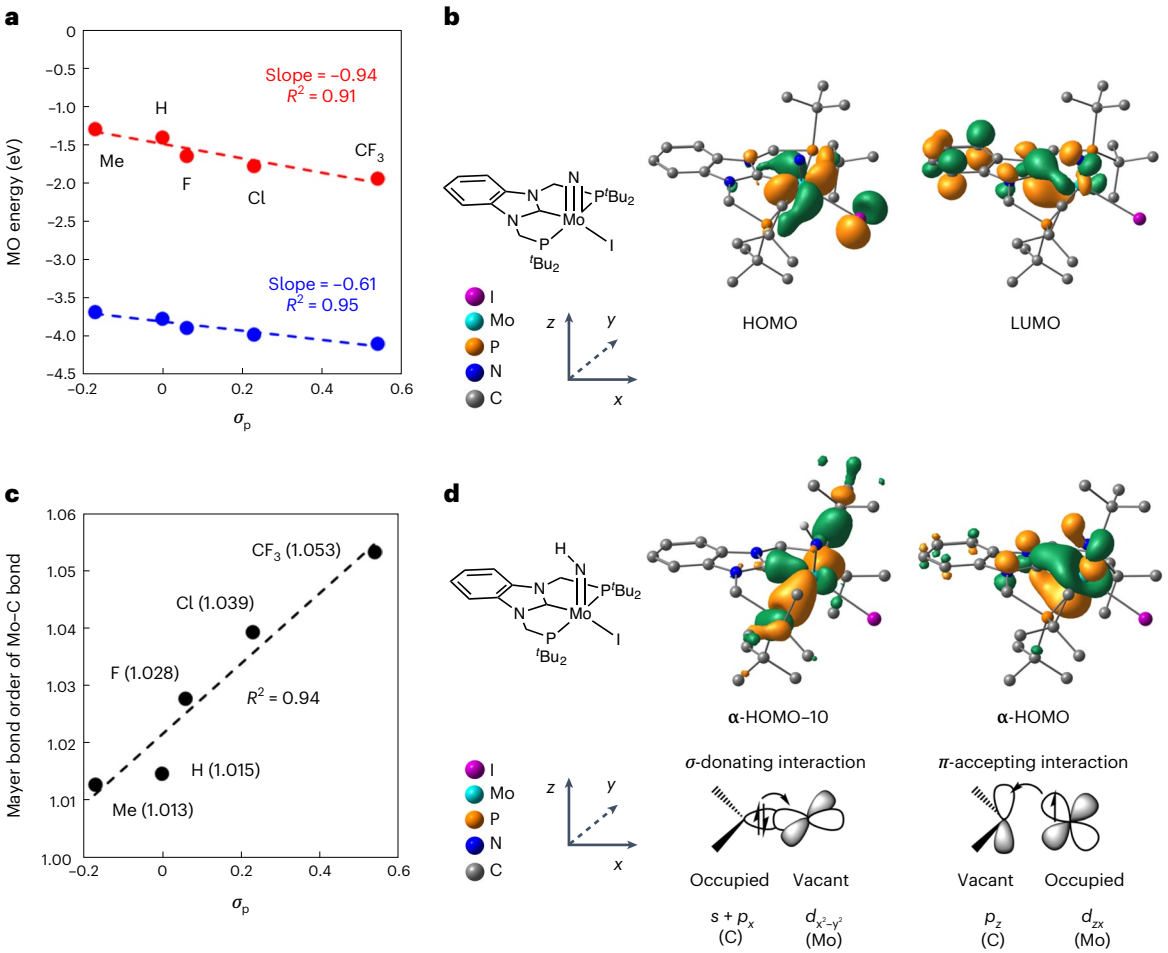

Fig. 3 | DFT calculations of molybdenum–nitride and molybdenum–imide complexes that bear PCP ligands. a, Energy plots of the LUMO (red) and HOMO (blue) energies of **2a** and the 5,6-substituted nitride complexes (**2b**–**2d** and **2f**) versus the Hammett substituent constant σ_p. **b**, Spatial distribution of the HOMO and LUMO of **2a**. **c**, Mayer bond orders of the Mo–C(carbene) of **Ia** and the 5,6-substituted imide complexes (**Ib**–**Id** and **If**) versus Hammett substituent constant σ_p. **d**, Spatial distribution and schematic drawings of frontier orbitals of **Ia** that contribute to the σ donation from the pincer ligand to Mo (α-HOMO-10) and the π backdonation from Mo to the pincer ligand (α-HOMO). MO, molecular orbital.

the PCP ligand would effectively lower the LUMO energy level. This increases the electron affinity of **2a**, which is essential to accelerate the rate-determining N–H bond formation reactions via PCET. In addition, the introduction of the electron-withdrawing substituents enhances the π-accepting ability of the PCP ligand, which leads to a solid connection between the Mo centre and the PCP ligand through π backdonation to give an improvement in the catalytic activity for nitrogen fixation.

Properties of the molybdenum complexes that bear PCP ligands

Based on the DFT results, we designed PCP-type pincer ligands that bear different substituents at positions 5 and/or 6 of the benzimidazole ring (**3a**–**3f**), as well as their corresponding molybdenum trichloride complexes [$MoCl_3$(R–PCP)] (**1a**–**1f**) (Fig. 4a,b, respectively). The electronic properties of these ligands and molybdenum complexes were estimated via NMR spectroscopy of the corresponding selenocarbene compounds of the PCP-type pincer ligands (**4a**–**4f**), the infrared spectroscopy of the corresponding molybdenum(0) tricarbonyl complexes that bear the same PCP-type pincer ligands, [$Mo(CO)_3$(R–PCP)] (**6a**–**6f**)[59,60] and the cyclic voltammetry of the isolated molybdenum(IV)–nitride complexes [Mo(N)I(R-PCP)] (**2a** and **2e**). The chemical shift of the ^{77}Se NMR spectra of the selenocarbene compounds generally reveals the π-backdonation ability of the corresponding carbene ligands[54,61]; the CO-stretching frequency of the carbonyl complexes measured via infrared spectroscopy reveals all the electronic properties of the pincer ligands, which includes those of carbene and two phosphine moieties. The redox potentials measured by cyclic voltammetry of the molybdenum(IV)–nitride complexes provide direct information on the electronic properties with regard to reactive intermediates.

First, we prepared the selenocarbene compounds (**4a**–**4f**) via the reactions of the corresponding carbene ligands with elemental selenium powder (see Supplementary Section 2 for the details) and performed ^{77}Se NMR spectroscopy of the corresponding selenocarbene compounds in THF-d_8 (Fig. 4a). The chemical shifts of the selenocarbene compounds, which were identified as selenium atoms that were bonded to carbon atoms, are listed in Table 2. The ^{77}Se NMR spectroscopy of the selenocarbene compounds revealed that the enhanced π backdonation contributes to the paramagnetic shielding term with a substantial downfield ^{77}Se-NMR signal[54,61]. The shift of the selenocarbene compounds that introduced two methyl groups as the electron-donating groups (**4b**, 135.2 ppm) was more upfield than that for the non-substituted selenocarbene compound (**4a**, 147.1 ppm). Contrarily, the introductions of the fluoro- (**4c**, 170.2 ppm), chloro- (**4d**, 177.3 ppm) and trifluoromethyl (**4e** and **4f** with one and two CF_3 groups, respectively, 174.3 and 196.6 ppm) groups as the electron-withdrawing groups facilitated downfield shifts. These results demonstrated that the π-backdonation ability

https://doi.org/10.1038/s44160-023-00292-9

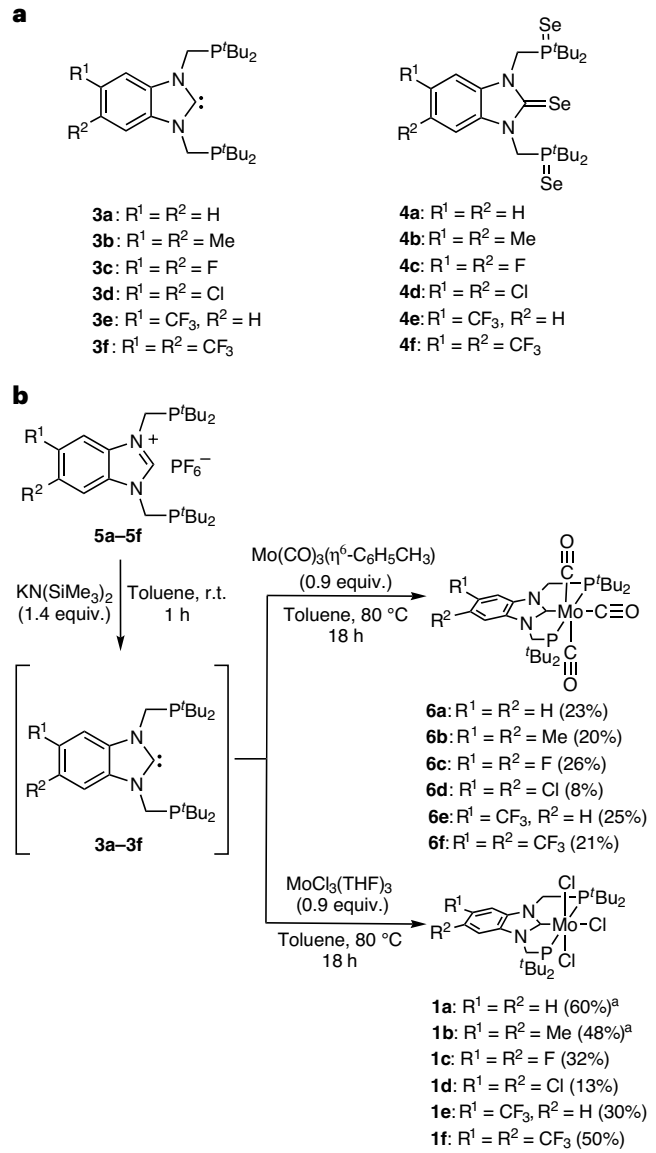

Fig. 4 | Preparation of the substituted PCP-type pincer ligands and their molybdenum complexes. a, Structures of the PCP-type pincer ligands that bear different substituents (**3a**–**3f**) and the corresponding selenocarbene compounds (**4a**–**4f**). **b**, Preparation of the molybdenum tricarbonyl and trichloro complexes that bear the PCP-type pincer ligands. [a]Reported data[29].

of the carbene moiety was effectively tuned via the introduction of substituent groups in positions 5 and/or 6 of the benzimidazole ring, as predicted by DFT.

Next, the molybdenum tricarbonyl complexes that bear the PCP-type pincer ligands, [Mo(CO)$_3$(R-PCP)] (**6a**–**6f**) were synthesized (Fig. 4b). The treatment of the pincer ligands (**3a**–**3f**), which were generated in situ via the reactions of the precursors of the PCP-pincer ligands (**5a**–**5f**) with 1.4 equiv. potassium hexamethyldisilazide (KN(SiMe$_3$)$_2$) in toluene for one hour at room temperature and 0.9 equiv. [Mo(CO)$_3$(η^6–C$_6$H$_5$CH$_3$)] in toluene for 18 hours at 80 °C yielded the corresponding molybdenum tricarbonyl complexes that bear the PCP-type pincer ligands, [Mo(CO)$_3$(R-PCP)] (**6a**–**6f**), in yields of 8–26%. X-ray analysis confirmed that the molecular structures of these complexes were almost the same (Supplementary Figs. 9–14). We measured the CO-stretching frequencies of **6a**–**6f** in a THF solution. Two signals, which corresponded to the CO-stretching frequency, were observed in all the complexes. A slightly smaller wavenumber of the CO-stretching frequency of **6b**, which introduced two methyl groups (1,831 and 1,935 cm^{-1}) as the electron-donating groups, than that of the non-substituted complex (**6a**, 1,833 and 1,936 cm^{-1}) was obtained. Conversely, the complexes that contained the fluoro-, chloro- and trifluoromethyl groups as electron-withdrawing groups exhibited higher wavenumbers (**6c**, 1,836 and 1,939 cm^{-1}; **6d**, 1,838 and 1,940 cm^{-1}; **6e**, 1,837 and 1,940 cm^{-1} and **6f**, 1,842 and 1,942 cm^{-1}). These infrared results indicated that the tendency of the effect of the substituent groups was consistent with that observed by NMR spectroscopy for the selenocarbene compounds (**4**), although we observed only a small difference in the CO-stretching frequencies of the molybdenum(0) tricarbonyl complexes (**6**) by the introduction of the substituent groups to positions 5 and/or 6 of the benzimidazole ring.

To obtain more detailed and direct information on the electronic property with regard to reactive intermediates, we measured the cyclic voltammetry of the molybdenum(IV)–nitride complex [Mo(N)I(PCP)] (**2a**). In this case, an irreversible reduction wave was observed at −2.85 V versus $FeCp_2^{+/0}$, which was estimated by differential pulse voltammetry measurements. However, in the case of the molybdenum(IV)–nitride complex that bear a CF$_3$-substituted PCP-type pincer ligand, [Mo(N)I(CF$_3$-PCP)] (**2e**), the comparable reduction potential shifted to −2.63 V versus $FeCp_2^{+/0}$ (Supplementary Fig. 1). These experimental results indicated that the introduction of electron-withdrawing groups, such as a CF$_3$ group at the 5-position in the PCP-type pincer ligand, substantially contributed to the electron-deficient molybdenum centre at the molybdenum(IV)–nitride complex. Thus, the electronic properties of the substituent groups that were introduced to positions 5 and/or 6 of the benzimidazole ring strongly affected the overall electronic properties of the pincer ligands.

We prepared molybdenum trichloro complexes that bear the PCP-type pincer ligands [MoCl$_3$(R-PCP)] (**1a**–**1f**) (Fig. 4b). The treatments of the pincer ligands **3c**–**3f**, which were generated in situ from the reactions of the precursors of the PCP-type pincer ligands **5c**–**5f**, respectively, with 0.9 equiv. [MoCl$_3$(THF)$_3$] in toluene for 18 hours at 80 °C, afforded the corresponding molybdenum trichloro complexes that bear the PCP-type pincer ligands [MoCl$_3$(R-PCP)] (**1c**–**1f**) in 13–60% yields. The molecular structures of **1c**–**1f** were confirmed by X-ray analysis (Supplementary Figs. 2–5). These complexes (**1c**–**1f**) exhibited solution magnetic moments of 3.8, 3.5, 3.8 and 3.9 μ_B, respectively, which indicates that these complexes were characterized by the S = 3/2 spin-state (3.87 μ_B) (see Supplementary Section 2 for the details).

Table 2 | Electronic properties of the substituted PCP-type pincer ligands and the catalytic production of ammonia with 1a–1f as the catalysts

Substituents of ligands (R^1, R^2)	^{77}Se-NMR chemical shifts of C=Se in 4[a]	TON (equiv. / Mo)[b]	TOF (equiv. / Mo min^{-1})[c]
(H, H)	147.1 (**4a**)	7,020±120	590±22
(Me, Me)	135.2 (**4b**)	5,350±560	320±12
(F, F)	170.2 (**4c**)	7,310±80	634±2
(Cl, Cl)	177.3 (**4d**)	8,170±230	620±81
(CF$_3$, H)	174.3 (**4e**)	8,480±340	798±48
(CF$_3$, CF$_3$)	196.6 (**4f**)	8,660±600	711±28

[a]^{77}Se NMR spectra were measured in THF-d_8, and the chemical shifts were referenced to an external standard ($SePh_2$). [b]TON values were calculated employing the amount of ammonia based on the Mo atom in the catalytic reaction after 60 min with **1a**–**1f**, respectively, as the catalysts, as shown in Fig. 5. Data are the mean of the multiple separate experiments (a minimum of two), and the error bars represent s.d. [c]TOF values were calculated employing the amount of ammonia based on the Mo atom in the catalytic reaction within 5 min with **1a**–**1f**, respectively, as the catalysts, as shown in Fig. 5. Data are the mean of the multiple separate experiments (a minimum of two), and the error bars represent s.d.

https://doi.org/10.1038/s44160-023-00292-9

a

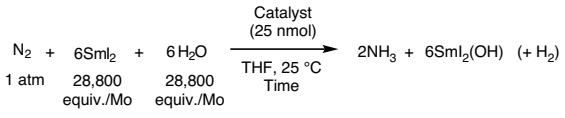

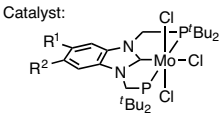

1a: $R^1 = R^2 = H$
1b: $R^1 = R^2 = Me$
1c: $R^1 = R^2 = F$
1d: $R^1 = R^2 = Cl$
1e: $R^1 = CF_3$, $R^2 = H$
1f: $R^1 = R^2 = CF_3$

b

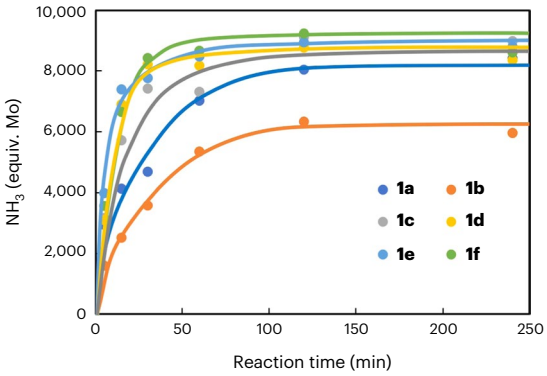

d

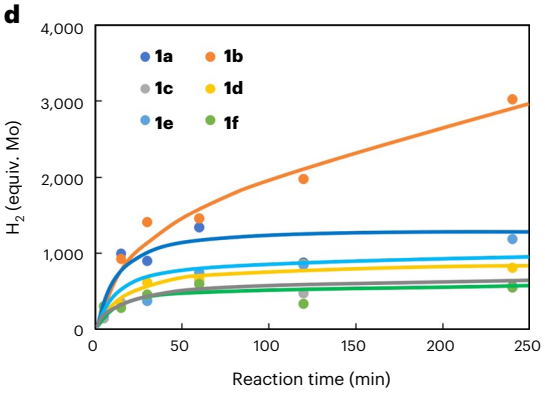

c

Catalyst	Reaction time (min) 5	15	30	60	120	240
1a	2,950 ± 110	4,130 ± 140	4,690 ± 330	7,020 ± 120	8,050 ± 300	8,410 ± 480
1b	1,600 ± 60	2,520 ± 850	3,580 ± 20	5,350 ± 560	6,330 ± 440	5,960 ± 560
1c	3,170 ± 10	5,730 ± 600	7,420 ± 280	7,310 ± 80	9,120 ± 70	8,990 ± 100
1d	3,100 ± 400	6,900 ± 120	8,220 ± 200	8,170 ± 230	8,770 ± 550	8,360 ± 410
1e	3,990 ± 240	7,400 ± 80	7,760 ± 410	8,480 ± 340	8,940 ± 80	8,800 ± 110
1f	3,560 ± 140	6,650 ± 520	8,430 ± 160	8,660 ± 600	9,240 ± 420	8,610 ± 290

e

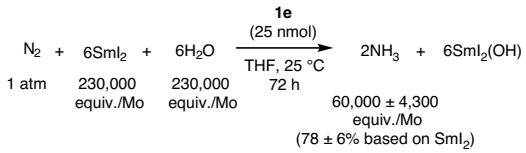

Fig. 5 | Time profiles of the catalytic production of ammonia catalysed by 1a–1f. a, Reaction conditions of the catalytic production of ammonia for the comparison of the catalytic activities of **1a**–**1f**. **b**, Time profiles of the amounts of ammonia produced from the catalytic production of ammonia catalysed by **1a**–**1f**. **c**, The data of panel **b** for the amounts of the ammonia (equiv. based on the Mo atom of the catalyst) that were produced by **1a**–**1f**. Data are means of multiple individual experiments (two to four times) with error bars based on s.d. **d**, Time profiles of the amounts of dihydrogen produced during the catalytic production of ammonia catalysed by **1a**–**1f** as a by-product. **e**, Catalytic reaction of dinitrogen (1 atm) with high amounts of SmI_2 and H_2O as the reductant and proton source, respectively.

Catalytic activities of the molybdenum PCP complexes

We examined the catalytic activities of **1a**–**1f** in the catalytic reduction of dinitrogen into ammonia by investigating the degree of progress of the catalytic reaction. The amount of ammonia produced from the reaction of dinitrogen with 28,800 equiv. SmI_2 as the reductant and 28,800 equiv. H_2O as the proton source in the presence of a catalytic amount (25 nmol) each of **1a**–**1f** in THF at 25 °C was measured in the reaction time range between five minutes and four hours (Fig. 5a). The time profiles of the amounts of ammonia in the catalytic reaction are shown in Fig. 5b,c. The amount of ammonia decreased significantly when a complex that bear two methyl groups, **1b**, was employed as the electron-donating group. Conversely, the utilization of complexes that bear the electron-withdrawing groups (**1c**–**1f**), as well as **1a**, accelerated the reaction in the early stage. The turnover number (TON) values, as calculated by the amount of ammonia based on the Mo atom in the reaction after 60 minutes, are presented in Table 2. Notably, the TON tended to increase as the electron-withdrawing strength of the substituents at positions 5 and/or 6 of the benzimidazole ring increased; maximum values were obtained in the presence of **1e** and **1f** as the catalysts. However, the TOFs, as calculated by the amount of ammonia based on the Mo atom in the reaction within five minutes (Table 2), slightly decreased when the complex (**1f**), which exhibited a stronger electron-withdrawing property than that of **1e** was utilized. Conversely, the amount of hydrogen gas produced as a by-product in this catalytic reaction system exhibited an inverse trend against the produced amount of ammonia when employing the catalysts (Fig. 5d). Thus, the amount of hydrogen gas increased significantly when the complex that bear two methyl groups was employed as the electron-donating groups (**1b**). The experimental results (Fig. 5) indicated that the DFT-based predictions of the designed molybdenum complexes as to the LUMO energies of the corresponding molybdenum–nitride complexes availed an efficient method to develop very effective molybdenum complexes as catalysts for the production of ammonia under ambient reaction conditions. In the present reaction system, the rate of ammonia formation decreased over time as reactants, such as SmI_2 and H_2O, were consumed after the start of the reaction. As a result, we consider that the reason for the decrease in the rate of ammonia formation over time is due to the consumption of reactants such as SmI_2 and H_2O. Thus, we do not believe that the reason is due to the effect of the produced ammonia and dihydrogen or the deactivation of the catalyst.

Finally, we conducted the catalytic reaction in the presence of **1e**, which exhibited the highest TON and TOF values among the prepared catalysts under the present reaction conditions higher amounts of the reductant and a proton source were employed (Fig. 5e). The reaction of dinitrogen (1 atm) with 230,000 equiv. each of SmI_2 and H_2O as the reductant and proton source, respectively, in the presence of a catalytic amount (25 nmol) of **1e** in THF for 72 hours at 25 °C was performed by adding the reductant and proton source in three portions. Therefore, 60,000 equiv. ammonia was obtained based on the Mo atom of the catalyst (with a yield of 78% based on SmI_2). This very high value is ~14 times

larger than our previously reported one (4,350 equiv. ammonia)[30], and the highest achieved among the catalytic activities of reported reactions that employed transition metal complexes as the catalysts.

Conclusion

In summary, we confirmed that molybdenum trichloride complexes bearing a trifluoromethyl-substituted PCP-type pincer ligand functioned as the most effective catalyst for the catalytic production of ammonia from dinitrogen under ambient reaction conditions based on the mechanistic insight afforded by the experimental results, as well as on the prediction of the DFT calculations on the reactive intermediates. In this novel reaction system, up to 60,000 equiv. ammonia were produced based on the Mo atom of the catalyst, demonstrating a TOF of up to 800 equiv. Mo min^{-1}. The amount of the ammonia produced in this study, as well as the production rate, were approximately one order of magnitude higher than those observed under previous reaction conditions[30].

As described in here, we consider that the use of the BDFE(N–H) values of key reactive intermediates, such as molybdenum–imide, molybdenum–amide and molybdenum–ammine complexes estimated by DFT calculations provides a suitable and reliable predicting method to develop more effective catalysts under ambient reaction conditions. The catalysts successfully developed will be applied not only to the catalytic nitrogen fixation driven by visible light[62] and electrochemical energy, but also to the catalytic formation of nitrogen-containing organic compounds directly from nitrogen gas under mild reaction conditions[63]. We believe that these findings can contribute to the development of an environmentally friendly next-generation nitrogen-fixation system in the near future.

Methods

In a 50 ml Schlenk flask was placed a CH_2Cl_2 solution of **1e** (0.05 mM, 500 µl, 25 nmol) and the solvent was removed under reduced pressure. To the flask were added $SmI_2(THF)_2$ (1.05 g, 1.92 mmol) and THF (6 ml) under N_2. Then a THF solution (1 ml) that contained H_2O (1.92 mmol) was added to the stirred solution in the Schlenk flask in one portion. After the addition of the water, the mixture was further stirred at 25 °C for 24 h. This procedure was then repeated twice (in total, $SmI_2(THF)_2$ (1.92 mmol × 3), H_2O (1.92 mmol × 3), 24 h × 3). Aqueous potassium hydroxide solution (30 wt%, 5 ml) was added to the reaction mixture. The mixture was evaporated under reduced pressure, and the distillate trapped in a dilute H_2SO_4 solution (0.5 M, 10 ml). The amount of ammonia (1.42 mmol, 56,800 equiv. based on the molybdenum atom, a 74% yield based on $SmI_2(THF)_2$) present in the H_2SO_4 solution was determined by the indophenol method.

Data availability

Source data are provided with this paper. The crystallographic data for **1c**·CH_2Cl_2, **1d**·0.5CH_2Cl_2, **1e**, **1f**, [Mo(N)I(PCP)]OTf, **2a**, **2e**, **6a**, **6b**, **6c**, **6d**, **6e**·C_4H_4O, and **6f** have been deposited with the Cambridge Crystallographic Data Centre under accession numbers 2069962, 2069963, 2069964, 2069965, 2069966, 2069967, 2222890, 2069968, 2069969, 2069970, 2069971, 2069972 and 2069973, respectively. The data supporting the findings of the current study are available within the paper and its Supplementary Information.

References

1. *Mineral Commodity Summaries 2021* (US Geological Survey, 2021).
2. Liu, H. *Ammonia Synthesis Catalysts: Innovation and Practice* (World Scientific, 2013).
3. Boerner, L. K. Taking the CO_2 out of NH_3. *Chem. Eng. News* **97**, 18–21 (2019).
4. Foster, S. L. et al. Catalysts for nitrogen reduction to ammonia. *Nat. Catal.* **1**, 490–500 (2018).
5. Valera-Medina, A., Xial, H., Owen-Jones, M., David, W. I. F. & Bowen, P. J. Ammonia for power. *Prog. Energy Combust. Sci.* **69**, 63–102 (2018).
6. Guo, J. & Chen, P. Catalyst: NH_3 as an energy carrier. *Chem* **3**, 709–712 (2017).
7. Ye, L., Nayak-Luke, R., Bañares-Alcántara, R. & Tsang, E. Reaction: 'green' ammonia production. *Chem* **3**, 712–714 (2017).
8. Service, R. F. Ammonia—a renewable fuel made from Sun, air, and water—could power the globe without carbon. *Science* https://doi.org/10.1126/science.aau748 (2018).
9. Marakatti, V. S. & Gaigneaux, E. M. Recent advances in heterogeneous catalysis for ammonia synthesis. *Chem. Cat. Chem.* **12**, 5838–5857 (2020).
10. Hosono, H. & Kitano, M. Advances in materials and applications of inorganic electrides. *Chem. Rev.* **121**, 3121–3185 (2021).
11. Hattori, M., Iijima, S., Nakao, T., Hosono, H. & Hara, M. Solid solution for catalytic ammonia synthesis from nitrogen and hydrogen gases at 50 °C. *Nat. Commun.* **11**, 2001 (2020).
12. Ye, T.-N. et al. Vacancy-enabled N_2 activation for ammonia synthesis on an Ni-loaded catalyst. *Nature* **583**, 391–395 (2020).
13. Yandulov, D. V. & Schrock, R. R. Catalytic reduction of dinitrogen to ammonia at a single molybdenum center. *Science* **301**, 76–78 (2003).
14. Nishibayashi, Y. *Nitrogen Fixation* (Topics in Organometallic Chemistry Vol. 60) (Springer, 2017).
15. Chalkley, M. J., Drover, M. W. & Peters, J. C. Catalytic N_2-to-NH_3 (or -N_2H_4) conversion by well-defined molecular coordination complexes. *Chem. Rev.* **120**, 5582–5636 (2020).
16. Masero, F., Perrin, M. A., Dey, S. & Mougel, V. Dinitrogen fixation: rationalizing strategies utilizing molecular complexes. *Chem. Eur. J.* **27**, 3892–3928 (2021).
17. Tanabe, Y. & Nishibayashi, Y. Comprehensive insights into synthetic nitrogen fixation assisted by molecular catalysts under ambient or mild conditions. *Chem. Soc. Rev.* **50**, 5201–5242 (2021).
18. Anderson, J. S., Rittle, J. & Peters, J. C. Catalytic conversion of nitrogen to ammonia by an iron model complex. *Nature* **501**, 84–87 (2013).
19. Hill, P. J., Doyle, L. R., Crawford, A. D., Myers, W. K. & Ashley, A. E. Selective catalytic reduction of N_2 to N_2H_4 by a simple Fe complex. *J. Am. Chem. Soc.* **138**, 13521–13524 (2016).
20. Fajardo, J. Jr. & Peters, J. C. Catalytic nitrogen-to-ammonia conversion by osmium and ruthenium complexes. *J. Am. Chem. Soc.* **139**, 16105–16108 (2017).
21. Doyle, L. R. et al. Catalytic dinitrogen reduction to ammonia at a triamidoamine–titanium complex. *Angew. Chem. Int. Ed.* **57**, 6314–6418 (2018).
22. Arashiba, K., Miyake, Y. & Nishibayashi, Y. A molybdenum complex bearing PNP-type pincer ligands leads to the catalytic reduction of dinitrogen into ammonia. *Nat. Chem.* **3**, 120–125 (2011).
23. Kuriyama, S. et al. Catalytic transformation of dinitrogen into ammonia and hydrazine by iron–dinitrogen complexes bearing pincer ligand. *Nat. Commun.* **7**, 12181 (2016).
24. Kuriyama, S. et al. Direct transformation of molecular dinitrogen into ammonia catalyzed by cobalt dinitrogen complexes bearing anionic PNP pincer ligands. *Angew. Chem. Int. Ed.* **55**, 14291–14295 (2016).
25. Sekiguchi, Y. et al. Catalytic reduction of molecular dinitrogen to ammonia and hydrazine using vanadium complexes. *Angew. Chem. Int. Ed.* **57**, 9064–9068 (2018).
26. Meng, F. et al. Ammonia formation catalyzed by dinitrogen-bridged dirhenium complex bearing PNP-pincer ligands under mild reaction conditions. *Angew. Chem. Int. Ed.* **60**, 13906–13912 (2021).

27. Ashida, Y. et al. Catalytic reduction of dinitrogen into ammonia and hydrazine using chromium complexes bearing PCP-type pincer ligand. *Chem. Eur. J.* **28**, e202200557 (2022).
28. Kuriyama, S. et al. Catalytic reduction of dinitrogen to ammonia and hydrazine using iron–dinitrogen complexes bearing anionic benzene-based PCP-type pincer ligands. *Bull. Chem. Soc. Jpn* **95**, 683–692 (2022).
29. Eizawa, A. et al. Remarkable catalytic activity of dinitrogen-bridged dimolybdenum complexes bearing NHC-based PCP-pincer ligands toward nitrogen fixation. *Nat. Commun.* **8**, 14874 (2017).
30. Ashida, Y., Arashiba, K., Nakajima, K. & Nishibayashi, Y. Molybdenum-catalysed ammonia production with samarium diiodide and alcohols or water. *Nature* **568**, 536–540 (2019).
31. Arashiba, K. et al. Catalytic nitrogen fixation via direct cleavage of nitrogen–nitrogen triple bond of molecular dinitrogen under ambient reaction conditions. *Bull. Chem. Soc. Jpn* **90**, 1111–1118 (2017).
32. Arashiba, K., Tanaka, H., Yoshizawa, K. & Nishibayashi, Y. Cycling between molybdenum–dinitrogen and –nitride complexes to support the reaction pathway for catalytic formation of ammonia from dinitrogen. *Chem. Eur. J.* **26**, 13383–13389 (2020).
33. Warren, J. J., Tronic, T. A. & Mayer, J. M. Thermochemistry of proton-coupled electron transfer reagents and its implications. *Chem. Rev.* **110**, 6961–7001 (2010).
34. Weinberg, D. R. et al. Proton-coupled electron transfer. *Chem. Rev.* **112**, 4016–4093 (2012).
35. Miller, D. C., Tarantino, K. T. & Knowles, R. R. Proton-coupled electron transfer in organic synthesis: fundamentals, applications, and opportunities. *Top. Curr. Chem.* **374**, 30 (2016).
36. Chciuk, T. V., Anderson, W. R. Jr & Flowers, R. A. II. Proton-coupled electron transfer in the reduction of carbonyls by samarium diiodide–water complexes. *J. Am. Chem. Soc.* **138**, 8738–8741 (2016).
37. Chciuk, T. V., Anderson, W. R. Jr & Flowers, R. A. II. Interplay between substrate and proton donor coordination in reductions of carbonyls by SmI_2–water through proton-coupled electron-transfer. *J. Am. Chem. Soc.* **140**, 15342–15352 (2018).
38. Kolmar, S. S. & Mayer, J. M. $SmI_2(H_2O)_n$ reduction of electron rich enamines by proton-coupled electron transfer. *J. Am. Chem. Soc.* **139**, 10687–10692 (2017).
39. Shaffer, D. W., Xie, Y., Szalda, D. J. & Concepcion, J. J. Manipulating the rate-limiting step in water oxidation catalysis by ruthenium bipyridine–dicarboxylate complexes. *Inorg. Chem.* **55**, 12024–12035 (2016).
40. Xie, Y., Shaffer, D. W. & Concepcion, J. J. O–O radical coupling: from detailed mechanistic understanding to enhanced water oxidation catalysis. *Inorg. Chem.* **57**, 10533–10542 (2018).
41. Bartulovich, C. O. & Flowers, R. A. II. Coordination-induced O–H bond weakening in Sm(II)–water complexes. *Dalton Trans.* **48**, 16142–16147 (2019).
42. Kuriyama, S. et al. Catalytic formation of ammonia from molecular dinitrogen by use of dinitrogen-bridged dimolybdenum–dinitrogen complexes bearing PNP-pincer ligands: remarkable effect of substituent at PNP-pincer ligand. *J. Am. Chem. Soc.* **136**, 9719–1931 (2014).
43. Itabashi, T. et al. Effect of substituents on molybdenum triiodide complexes bearing PNP-type pincer ligands toward catalytic nitrogen fixation. *Dalton Trans.* **48**, 3182–3186 (2019).
44. Becke, A. D. Density-functional exchange-energy approximation with correct asymptotic behavior. *Phys. Rev. A* **38**, 3098–3100 (1988).
45. Becke, A. D. Density-functional thermochemistry. III. The role of exact exchange. *J. Chem. Phys.* **98**, 5648–5652 (1993).
46. Lee, C., Yang, W. & Parr, R. G. Development of the Colle–Salvetti correlation-energy formula into a functional of the electron density. *Phys. Rev. B* **37**, 785–789 (1988).
47. Vosko, S. H., Wilk, L. & Nusair, M. J. Accurate spin-dependent electron liquid correlation energies for local spin density calculations: a critical analysis. *Can. J. Phys.* **58**, 1200–1211 (1980).
48. Grimme, S., Antony, J., Ehrlich, S. & Krieg, H. A consistent and accurate ab initio parametrization of density functional dispersion correction (DFT-D) for the 94 elements H–Pu. *J. Phys. Chem.* **132**, 154104 (2010).
49. Wang, D., Loose, F., Chirik, P. J. & Knowles, R. R. N–H bond formation in a manganese(V) nitride yields ammonia by light-driven proton-coupled electron transfer. *J. Am. Chem. Soc.* **141**, 4795–4799 (2019).
50. Loose, F. et al. Evaluation of excited state bond weakening for ammonia synthesis from a manganese nitride: stepwise proton coupled electron transfer is preferred over hydrogen atom transfer. *Chem. Commun.* **55**, 5595–5598 (2019).
51. Park, Y. et al. Visible light enables catalytic formation of weak chemical bonds with molecular hydrogen. *Nat. Chem.* **13**, 969–976 (2021).
52. Ashida, Y. et al. Molybdenum-catalyzed ammonia formation using simple monodentate and bidentate phosphines as auxiliary ligands. *Inorg. Chem.* **58**, 8927–8932 (2019).
53. Boekell, N. G. & Flowers, R. A. II. Coordination-induced bond weakening. *Chem. Rev.* **122**, 13447–13477 (2022).
54. Hansch, C., Leo, A. & Taft, R. W. A survey of Hammett substituent constants and resonance and field parameters. *Chem. Rev.* **91**, 165–195 (1991).
55. Verlinden, K., Buhl, H., Frank, W. & Ganter, C. Determining the ligand properties of N-heterocyclic carbenes from ^{77}Se NMR parameters. *Eur. J. Inorg. Chem.* **2015**, 2416–2425 (2015).
56. Vummaleti, S. V. C. et al. What can NMR spectroscopy of selenoureas and phosphinidenes teach us about the N-accepting abilities of N-heterocyclic carbenes? *Chem. Sci.* **6**, 1895–1904 (2015).
57. Mayer, I. Charge, bond order and valence in the ab initio SCF theory. *Chem. Phys. Lett.* **97**, 270–274 (1983).
58. Egi, A., Tanaka, H., Konomi, A., Nishibayashi, Y. & Yoshizawa, K. Nitrogen fixation catalyzed by dinitrogen-bridged dimolybdenum complexes bearing PCP- and PNP-type pincer ligands: a shortcut pathway deduced from free energy profiles. *Eur. J. Inorg. Chem.* **2020**, 1490–1498 (2020).
59. Nelson, D. J. & Nolan, S. P. Quantifying and understanding the electronic properties of N-heterocyclic carbenes. *Chem. Soc. Rev.* **42**, 6723–6753 (2013).
60. Huynh, H. V. Electronic properties of N-heterocyclic carbenes and their experimental determination. *Chem. Rev.* **118**, 9457–9492 (2018).
61. Liske, A., Verlinden, K., Buhl, H., Schaper, K. & Ganter, C. Determining the π-acceptor properties of N-heterocyclic carbenes by measuring the ^{77}Se NMR chemical shifts of their selenium adducts. *Organometallics* **32**, 5269–5272 (2013).
62. Ashida, Y. et al. Catalytic nitrogen fixation using visible light energy. *Nat. Commun.* **13**, 7263 (2022).
63. Itabashi, T. et al. Direct synthesis of cyanate anion from dinitrogen catalysed by molybdenum complexes bearing pincer-type ligand. *Nat. Commun.* **13**, 6161 (2022).

Acknowledgements

This project was supported by CREST, JST (JPMJCR1541). We acknowledge the Grants-in-Aid for Scientific Research (nos. JP20H05671, JP20K21203 and 22K19041) from JSPS and MEXT. Y.A. is a recipient of the JSPS Research Fellowships for Young Scientists. This paper is based on results obtained from project

JPNP21020 commissioned by the New Energy and Industrial Technology Development Organization (NEDO).

Author contributions

Y.N. and K.Y. conceived and designed this project. T.M., Y.A. and K.A. conducted the experimental work, which included the X-ray analysis. H.T. and A.E. conducted the theoretical studies. All the authors discussed the results and drafted the manuscript.

Competing interests

Y.A., K.A. and Y.N. have filed patents based on the research reported here (Japanese patent application nos. 2018-158595, 2018-036967 and 2018-036967 and international patent application JP2019/007793). The remaining authors declare no competing interests.

Additional information

Supplementary information The online version contains supplementary material available at https://doi.org/10.1038/s44160-023-00292-9.

Correspondence and requests for materials should be addressed to Kazunari Yoshizawa or Yoshiaki Nishibayashi.

Peer review information *Nature Synthesis* thanks the anonymous reviewers for their contribution to the peer review of this work. Primary Handling Editor: Peter Seavill, in collaboration with the *Nature Synthesis* team.